Tracing seasonal signals in dry/wet status for regions with simultaneous rain and heat from Eastern and Central Asia since the Last Glacial Maximum

Simin Peng[1], Yu Li[1], Zhansen Zhang[1], Mingjun Gao[1], Xiaowen Chen[1], Junjie Duan[1], Yaxin Xue[1]

[1]Key Laboratory of Western China's Environmental Systems (Ministry of Education), College of Earth and Environmental Sciences, Center for Hydrologic Cycle and Water Resources in Arid Region, Lanzhou University, China

Correspondence to: Yu Li (liyu@lzu.edu.cn)

Abstract. The global monsoon region with the summer precipitation regime and the Mediterranean climate region with the winter precipitation regime show opposite dry/wet evolution since the Last Glacial Maximum (LGM). Therefore, different precipitation regimes bring about the contradiction in dry/wet status between Eastern and Central Asia (EA and CA). Based on the comprehensive study of modern observation datasets, ensemble simulations of eight climate models from the Paleoclimate Model Intercomparison Project phase 3 (PMIP3), and the compilation of 42 proxy records from EA and CA, here we reveal that seasonal signals of precipitation derived from the simultaneity of rain and heat periods could govern the difference and linkage in dry/wet status from EA and CA. At short-term timescales, EOF analysis results of mean annual precipitation uncover the spatial diversity of overall precipitation pattern in EA and CA. However, EOF results of summer and winter precipitation indicate the similarity between EA and the east of CA, suggesting that seasonal signals of precipitation affected by the Asian monsoon, westerlies, ENSO, NAO, and PDO are the primary factor causing the linkage in dry/wet status. At long-term timescales, proxy records since the LGM in EA and CA reveal parallel dry/wet evolution in EA and the east of CA as well. A visual inspection from PMIP3 multi-model simulations in summer and winter shows that the insolation in different seasons control the intensity of westerlies and summer monsoon and further influence the summer and winter precipitation in EA and CA since the LGM. Overall, we suggest, in addition to the traditional difference caused by different precipitation regimes, that dry/wet status in EA and CA universally have inter-regional connections affected by seasonal signals of precipitation at multi-time scales.

1 Introduction

As typical midlatitude climatic regions, Eastern and Central Asia (EA and CA) are commonly featured with vigorous circulations and are dominated by two atmospheric systems, namely midlatitude westerlies and Asian monsoon (Li, 1990; Zhang and Lin, 1992; Chen et al., 2008; Nagashima et al., 2011). These two regions are generally characterized by opposite climate and environment changes, embodied in water resources, vegetation cover and ecosystems, which gives rise to their different response to climate change (Sorg et al., 2012; Zhang and Feng, 2018). CA, where precipitation is scarce throughout

30   the year, is the largest arid region in the mid-latitudes dominated by westerlies (Chen et al., 2009; Huang et al., 2015a). On the contrary, affected by the Asian summer monsoon that carries water vapor from the Ocean, the monsoon-dominated EA has more precipitation (Wang et al., 2017). These contrasting climate regimes have attracted much research interest.

Over the past few years, there have been many comparative studies for dry/wet changes in EA and CA at multi-time scales, e.g., orbital, millennial, interdecadal timescales and annual timescales. Early works suggested that the climate change mode of

35   'cold-wet' or 'warm-dry' occurred in northwestern China during the last glacial/interglacial cycle, which is different from the 'cold-dry' or 'warm-wet' modes of the monsoon climate (Li, 1990; Han and Qu, 1992; Han et al., 1993). In monsoonal EA, a strengthened summer monsoon and humid climate usually occur in the early and mid Holocene, and a weakened summer monsoon and drier climate prevailed during the late Holocene (Dykoski et al., 2005; Chen et al., 2015). Based on the integration of paleoclimate records, modern meteorological observation data and paleoclimate simulations, Chen et al. (2008, 2009, 2019)

40   revealed that the 'westerlies-dominated climatic regime' in arid CA presents dry early Holocene, wetter mid-Holocene, and moderately wet late Holocene, which is out-of-phase or anti-phased with the dry/wet status in the monsoon-dominated regions. However, the paleoclimate records in some regions of CA provided asynchronous climate evolution history, in contradiction with the dry/wet changes caused by the westerlies (An et al., 2006; Zhao et al., 2015; Wang et al., 2018). The latest studies proposed that the persistent weakening of the East Asian summer monsoon since 1958 causes an increasing contribution of the

45   monsoonal water vapor transport, thereby enhancing summer precipitation in arid CA on the annual timescale (Chen et al., 2021a; Chen et al., 2021b). Therefore, further research is needed to explain dry/wet changes in different regions and explore the difference and linkage in climate change modes from EA and CA at multi-time scales.

The seasonal signals of precipitation, derived from the simultaneity of rain and heat periods, is an important climate phenomenon at the multi-time scale. It behaves as that the summer half-year at short-term timescales and warm period at long-

50   term timescales get more precipitation than the winter half-year and cold period respectively. This study aims to focus on the transitional zone in the arid and semi-arid region of eastern CA where the westerlies and the monsoon interact and have the summer precipitation regime the same as the monsoon-dominated EA. Utilizing modern observations, paleoclimate proxies, and model simulations, we conducted a comprehensive analysis for dry/wet status in EA and CA on multi-time scales based on seasonal signals of precipitation.

55   **2 Materials and methods**

2.1 Study area

In this study, we divide the boundaries of CA and EA mainly according to the modern Asian summer monsoon limit designed by Chen et al. (2008, 2019). CA is the largest arid and semi-arid areas in the mid-latitude hinterland of the Eurasian continent, extending from the Caspian Sea in the west to the modern Asian summer monsoon limit in the east, comprising the central

60　Asian countries, NW China, and southern Mongolian Plateau (Fig. 1). Considering that the strength and trajectory of monsoon circulation is a major control on moisture in EA, we viewed Chinese monsoon region in the east and south of the modern Asian summer monsoon limit in China as EA (Fig. 1). We calculated the precipitation difference between the summer (April, May, June, July, August, and September) and winter (January, February, March, October, November, and December) half year over 1971-2020, and then defined the region greater than 0 mm as the simultaneous region of rain and heat periods. Therefore, we

65　define the simultaneous region of rain and heat periods in CA as the east of CA (Fig. 1). The seasonality perspective implies that different precipitation regimes could affect the difference and linkage in climate change modes from EA and CA at the multi-time scale. Taking seasonal signals as the dividing criteria, the core region of CA is characterized by a wet cold-season climate, whereas EA and the east of CA are characterized by a wet warm-season climate (Fig. 1).
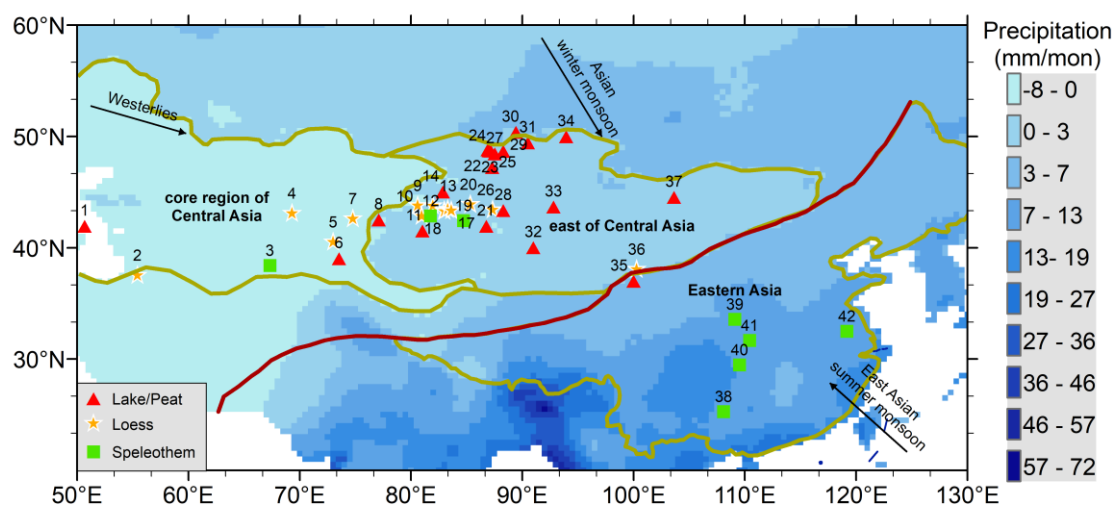
Figure 1. Overview map showing the paleoclimate record sites selected in this study from EA and CA, the difference between summer and winter precipitation over 1965-2014 (shade), and the dominant circulation systems, including the westerlies, Asian winter monsoon and East Asian summer monsoon. The modern Asian summer monsoon limit (red solid line) is summarized by Chen et al. (2008, 2019). The gray slash represents the simultaneous region of the rain and heat periods. The brown solid line represents the range of CA, the core region of CA, the east of CA, and EA as defined in this study.

75　**2.2 Modern observation and analytical methods**

The monthly high-resolution (0.5°×0.5°) land precipitation data (referred to as CRU TS4.06) are selected from a Climatic Research Unit (CRU) updated gridded climate dataset in the University of East Anglia (van der Schrier et al., 2013; Harris et al., 2014; Barichivich et al., 2021). The CRU monthly climate archives are obtained from the auspices of the World Meteorological Organization (WMO) in league with the US National Oceanographic and Atmospheric Administration (NOAA,

80　via its National Climatic Data Center, NCDC). Global Reanalysis 1 dataset including monthly mean geopotential height, zonal wind, and meridional wind is collected from the National Centers for Environmental Prediction/National Center for Atmospheric Research (NCEP/NCAR) (Kalnay et al., 1996). The reanalysis datasets have a horizontal resolution of 2.5° in latitude and longitude and a vertical resolution of 17 pressure levels from 1000 to 10 hPa. The high-resolution monthly

averaged data for the vertical integral water vapor from the European Centre for Medium-Range Weather Forecasts (ECMWF) reanalysis v5 (ERA5), intending to be used as a meteorological forcing dataset for land surface and hydrological models, is used in this study. This dataset is from 1979 to the present with a spatial resolution of 0.25° in latitude and longitude and a single level integrated from the surface to the top of the atmosphere (Hersbach et al., 2020).

We used the National Centers for Environmental Information (NCEI) Pacific Decadal Oscillation (PDO) index based on NOAA's extended reconstruction of SSTs (ERSST Version 5) to analyze long-lived El Niño-like pattern of Pacific climate variability (Zhang et al. 1997; Mantua and Hare, 2002). The data can be obtained at https://www.ncei.noaa.gov/pub/data/cmb/ersst/v5/index/ersst.v5.pdo.dat. The Niño 3.4 index is the most commonly used index to define El Niño and La Niña events. We selected the Niño 3.4 of area-averaged SST from 5°S-5°N and 170-120°W using the HadISST1 dataset (Rayner et al., 2003). The data can be obtained at https://psl.noaa.gov/gcos_wgsp/Timeseries/Nino34/. Positive values of the North Atlantic Oscillation (NAO) index are typically associated with stronger midlatitude westerlies and increased water vapor content from the North Atlantic. We used the Hurrell NAO index (station-based) to investigate the impact of NAO on midlatitude westerlies (Hurrell, 1995; Hurrell and Deser, 2009). The data can be obtained at https://climatedataguide.ucar.edu/sites/default/files/2022-10/nao_station_monthly.txt.

Empirical orthogonal function (EOF) is a powerful method for dimensionality reduction and pattern extraction. EOF can decompose multidimensional climate data from different locations into spatial (EOF modes) and temporal functions (principal components). Therefore, to investigate the spatiotemporal variations of precipitation at the interannual timescale over EA and CA, the EOF analysis was applied to the CRU TS4.06 gridded precipitation data and ERA5 vertical integral water vapor. We focused on the first two leading modes that objectively account for the majority of dry/wet status in EA and CA (Lorenz, 1956).

2.3 Calculation of Monsoon and westerly wind indices

The East Asian summer monsoon index (EASMI) is defined as the 850 hPa average summer meridional wind speed from June to August over (27°N~37°N, 110°E~120°E) encompassing the East Asian summer monsoon domain (Liu et al., 2014). The equation is as follows:

$$\text{EASMI} = \overrightarrow{V_{850}}(27°\sim37°\text{N}, 110°\sim120°\text{E}) \tag{1}$$

The westerly wind index (WWI) is defined as the zonal difference of the 500 hPa averaged geopotential height over (35°N~50°N, 70°E~110°E) (Li et al., 2008). The equation is as follows:

$$\text{WWI} = \overline{H_{35°}} - \overline{H_{50°}} = \frac{1}{17}\left[\sum_{\gamma=1}^{17} H(\gamma, 35°\text{N}) - \sum_{\gamma=1}^{17} H(\gamma, 50°\text{N})\right] \tag{2}$$

where H is the 500 hPa average height geopotential, γ is the number of longitudes taken along the latitude circle with a spacing of 2.5°.

The East Asian winter monsoon index (EAWMI) is defined as the difference between the 300 hPa averaged zonal wind speed from December to February over (27.5°~37.5°N, 110°~170°E) and (50°~60°N, 80°~140°E) (Jhun and Lee, 2004). The equation is as follows:

$$\text{EAWMI} = \overrightarrow{U_{300}}(27.5°\!\sim\!37.5°N, 110°\!\sim\!170°E) - \overrightarrow{U_{300}}(50°\!\sim\!60°N, 80°\!\sim\!140°E) \tag{3}$$

The calculation of EASMI, WWI, and EAWMI all rely on the NCEP Reanalysis 1 dataset.

2.4 Regional paleoclimatic proxy data

Here we compiled various paleoclimate records to reconstruct long-term climate variability and primarily paid close attention to paleo-precipitation and moisture changes since the LGM. We set three criteria to collect all the published proxy records from EA and CA in our study. Firstly, the records should be located primarily in the intersection encompassing the simultaneous region of rain and heat periods in EA and CA, which is in favor of investigating the difference and linkage in climate change modes from EA and CA. Accordingly, some typical records climatologically influenced by midlatitude westerlies and East Asian summer monsoon in core regions of CA and EA were selected for comparative analysis. Secondly, the proxies should be clearly indicative of changes in effective moisture or precipitation which have been confirmed by the original investigators. Third, the record length should cover the most period since LGM without documented depositional hiatuses. Fourth, the fluctuation and variation of proxy records should be predominantly forced by climate change, rather than human activities (Manoj et al., 2020; Chen et al., 2021c, 2022). Following the above criteria, a total of 42 proxy records from lakes, peats, loess, and stalagmites since the LGM were compiled for EA and CA (Fig. 1), enabling us to comprehensively review the LGM moisture evolution of the region. In light of seasonal signals of precipitation, 35 records are from the summer precipitation region, and seven records are from the winter precipitation region. Detailed information about these selected proxy records is presented in Table S1.

2.5 Paleoclimatic simulations

The Paleoclimate Modeling Intercomparison Project (PMIP) was launched to coordinate and encourage the systematic study of General Circulation Models (GCMs) and to understand the mechanisms of climate change and the role of climate feedback (Joussaume et al., 1999) (Table 1). Eight coupled GCMs covering the LGM or MH from the PMIP3 database were selected to analyze the mechanisms of climate change in this study (Table 2), including bcc-csm1-1, CNRM-CM5, CCSM4, CSIRO-Mk3-6-0, GISS-E2-R, MIROC-ESM, FGOALS-s2, and MRI-CGCM3. The output data of the PMIP3 in the LGM and MH are available at htQTPs://esgf-node.llnl.gov/search/esgf-llnl/. By chiefly interpolating various climate variables on the common 1°×1° grid and then sorting the values of model simulations from minimum to maximum, we extracted the median value of all PMIP3 models used in this paper to evaluate the PMIP3 model simulations and acquire the scientific model simulation value.

Table 1. Boundary conditions and forcing for PMIP3-CMIP5 models at the LGM and MH.

Period	Eccentricity	Obliquity (°)	Longitude of perihelion (°)	CO_2 (ppm)	CH_4 (ppb)	N_2O (ppb)	Ice sheet	Vegetation
LGM	0.018994	22.949	114.425	185	350	200	Peltier (2004), 21 ka	Present day
MH	0.018682	24.105	0.87	280	650	270	Peltier (2004), 0 ka	Present day

Table 2. Basic information about climate models from PMIP3-CMIP5 used in this study.

Model	Institute	Resolutions	Variables[*]	References
bcc-csm1-1	Beijing Climate Center, China Meteorological Administration, China	64×128 (17)	ua, va, zg, hus, psl, pr, tas	Randall et al. (2007)
CNRM-CM5	Centre National de Recherches Météorologiques, France	128×256 (17)	ua, va, zg, hus, psl, pr, tas	Voldoire et al. (2013)
CCSM4	National Center for Atmospheric Research, USA	288×192 (17)	ua, va, zg, hus, psl, pr, tas	Gent et al. (2011)
CSIRO-Mk3-6-0	Australian Commonwealth Scientific and Industrial Research Organization Marine and Atmospheric Research in collaboration with the Queensland Climate Change Centre of Excellence, Australia	96×192 (18)	ua, va, zg, hus, psl, pr, tas	Rotstayn et al. (2010)
GISS-E2-R	NASA Goddard Institute for Space Studies, USA	144×90 (17)	ua, va, zg, hus, psl, pr, tas	Schmidt et al. (2014)
MIROC-ESM	Japan Agency for Marine-Earth Science and Technology, Japan	128×64 (35)	ua, va, zg, hus, psl, pr, tas	Watanabe et al. (2011)
FGOALS-s2	LASG-CEES. China	108×128 (17)	ua, va, zg, hus, psl, pr, tas	Briegleb et a1. (2004)
MRI-CGCM3	Meteorological Research Institute, Japan	320×160 (23)	ua, va, zg, hus, psl, pr, tas	Yukimoto et al. (2012)

145 [*]: ua means eastward_wind; va means northward wind; zg geopotential Height; hus near-surface relative humidity; psl means sea surface pressure; pr means precipitation; tas means near-surface temperature.

3 Results

3.1 Seasonal signals at short-term timescales

To obtain the spatial distribution characteristics of the precipitation anomalies in EA and CA under the context of seasonal

150 signals, we conducted an EOF analysis on the precipitation standardized anomaly field over 1971-2020. Figure S1a-d shows

the spatial distribution and time series of EOF decomposition of mean annual precipitation. The center of negative values is in the core region of CA mainly belonging to the winter precipitation regime, while the positive values are in the south and north of EA located in summer precipitation regions (Fig. S1a). This opposite distribution indicates that the difference in the mean annual precipitation exists between EA and CA. Additionally, the first mode exhibits interdecadal and interannual changes

155 according to the PC1 (Fig. S1b). The second mode indicates that the center of positive values is in the north of EA, and the center of negative values is in the north of CA, also displaying the spatial diversity of mean annual precipitation in EA and CA (Fig. S1c).

In order to further explore the contribution of seasonal signals of precipitation to dry/wet status in EA and CA, we conducted EOF analysis on spring, summer, autumn, and winter precipitation data. The variance contribution rate of the first mode in

160 precipitation of four seasons is shown in Fig. 2. The first mode of spring and autumn precipitation does not show obvious distribution characteristics, and the contribution rate is relatively uniform, indicating that spring and autumn precipitation have no special precipitation contribution to EA and CA (Fig. 2a and c). In summer precipitation, the centers of positive values are mainly distributed in the north of EA and the east of CA, while the negative values are mainly distributed in the core regions of CA and center of EA (Fig. 2b). But similar EOF results between CA and south of EA do not exist in winter precipitation.

165 These spatial distribution indicates that summer precipitation mainly affects the dry/wet status in north of EA and the east of CA belonging to the simultaneous region of rain and heat periods, which is in contrast to the core region of CA. In winter precipitation, the center of the positive value is located in the core region of CA and north of EA, showing the significant contribution of winter precipitation to CA (Fig. 2d). It is worth noting that a certain degree of similarities exists in both summer and winter precipitation of EA and CA, indicating the impact of seasonal precipitation on the linkage of dry/wet status in EA

170 and CA at short-term timescales.
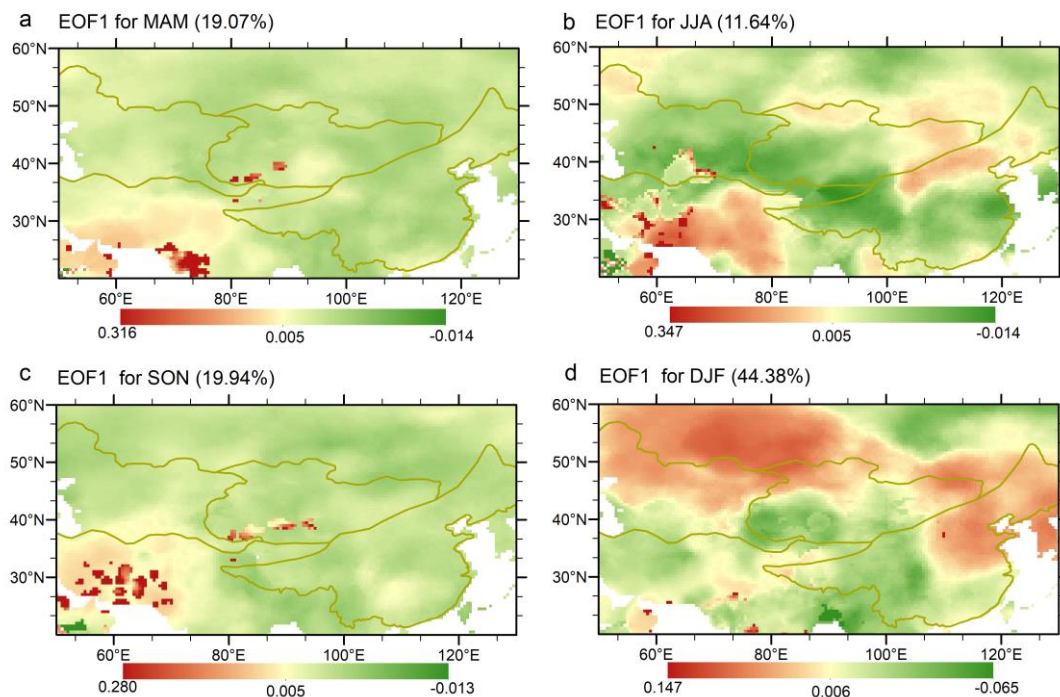
Figure 2. The first EOF modes of precipitation in spring (March, April, and May, MAM) (a), summer (June, July, and August, JJA) (b), autumn (September, October, and November, SON) (c), and winter (December, January, and February, DJF) (d) in EA and CA over 1971-2020.

Existing studies emphasized the role of water vapor sources in affecting interannual to interdecadal variability of precipitation (Chen and Huang, 2012; Huang et al., 2015a; Peng and Zhou, 2017; Wei et al., 2017). Therefore, by analyzing the EOF results of water vapor content in the whole layer, this study investigates the general characteristics of the spatial distribution of water vapor in EA and CA and discusses the influence mechanism of seasonal signals on dry/wet status in EA and CA at short-term timescales. The EOF1 of the mean annual water vapor shows that the core region of CA is dominated by positive values, while EA and the east of CA are synchronized with negative values (Fig. 3a). The same spatial distribution mode is also reflected in the EOF1 of water vapor difference between summer and winter half-year. To summarize, the water vapor in EA and CA shows a dipole out-of-phase pattern between the simultaneous region of rain and heat periods and the non-simultaneous region of rain and heat periods (Fig. 3b). This implies that the content and source of water vapor are the important reason why the dry/wet status in the east of CA is linked to that in EA by seasonal signals of precipitation.
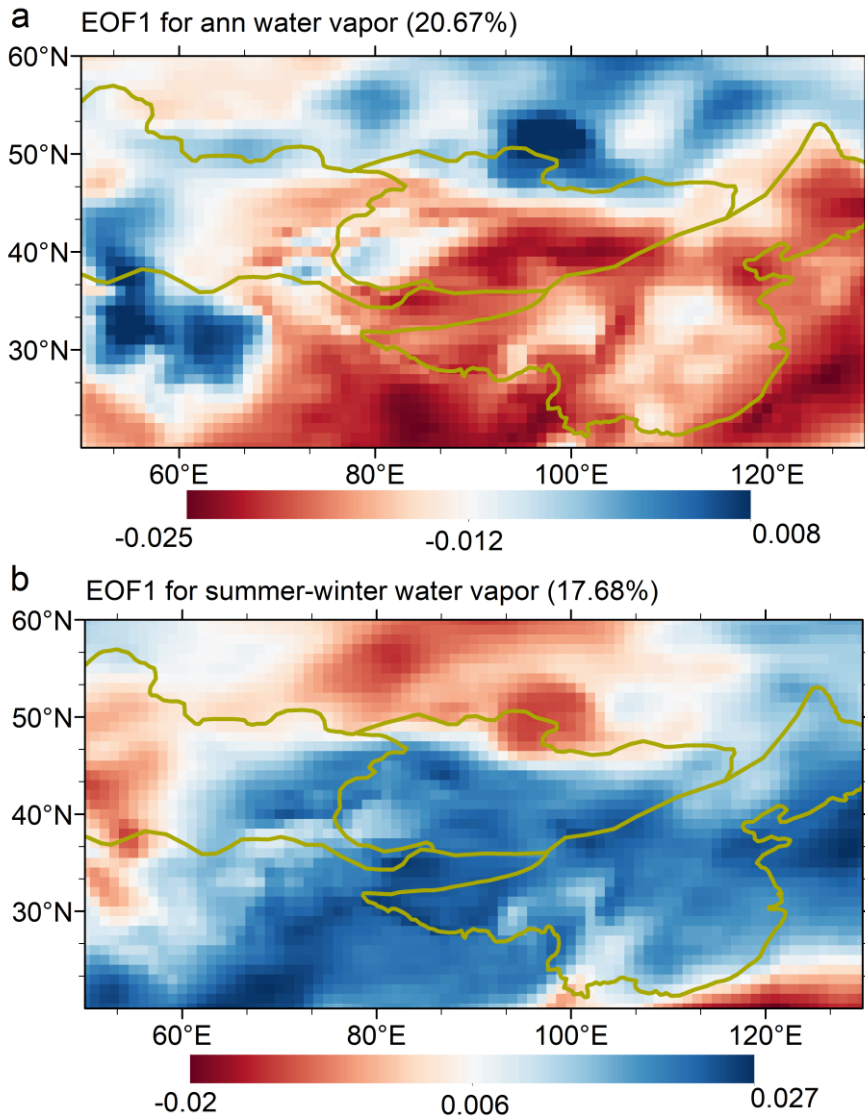

Figure 3. a, the EOF1 modes of annual mean integral water vapor in EA and CA over 1979-2018; b, the EOF1 modes of integral water vapor difference between summer and winter in EA and CA over 1979-2018.

3.2 Spatiotemporal variation of dry/wet status and seasonal signals at long-term timescales

In the last decade, many paleoclimate records with a relatively high resolution, reliable chronology, and unambiguous proxies have been published to discuss the long-term timescale climate evolution in EA and CA. Forty-two moisture records from individual sites are used to illustrate the spatiotemporal pattern of dry/wet status since the LGM in EA and CA (Fig. 4). During the LGM, most regions in EA and CA are in moderately dry condition (Fig. 4a). However, moderately wet and wet conditions partly exist in the east of CA. According to the model simulation, Yu et al. (2000) concluded that the low temperature in the cold period causes decreasing evaporation, with the enhanced westerlies driven by expanding land ice sheets, forming the high lake level in western China and the low lake level in eastern China during the LGM. During the early Holocene (EH), CA was dominated by a dry climate, while EA was moderately wet (Fig. 4b). At the same time, there were many records in the east of CA similar to the dry/wet status of EA. During the MH, the dry/wet status is mainly wet in the core region of CA and gradually turns into moderately wet and even dry conditions in the east of CA, while the EA remains moderately wet (Fig. 4c). By the late Holocene (LH), the EA is characterized by dry status, while CA is wet (Fig. 4d). In particular, the dry condition during the LGM and the wet climate during the EH and MH also reflect another meaning of seasonal signals derived from the simultaneity of rain and heat periods at long-term timescales, namely the "dry-cold" pattern and "wet-warm" pattern.
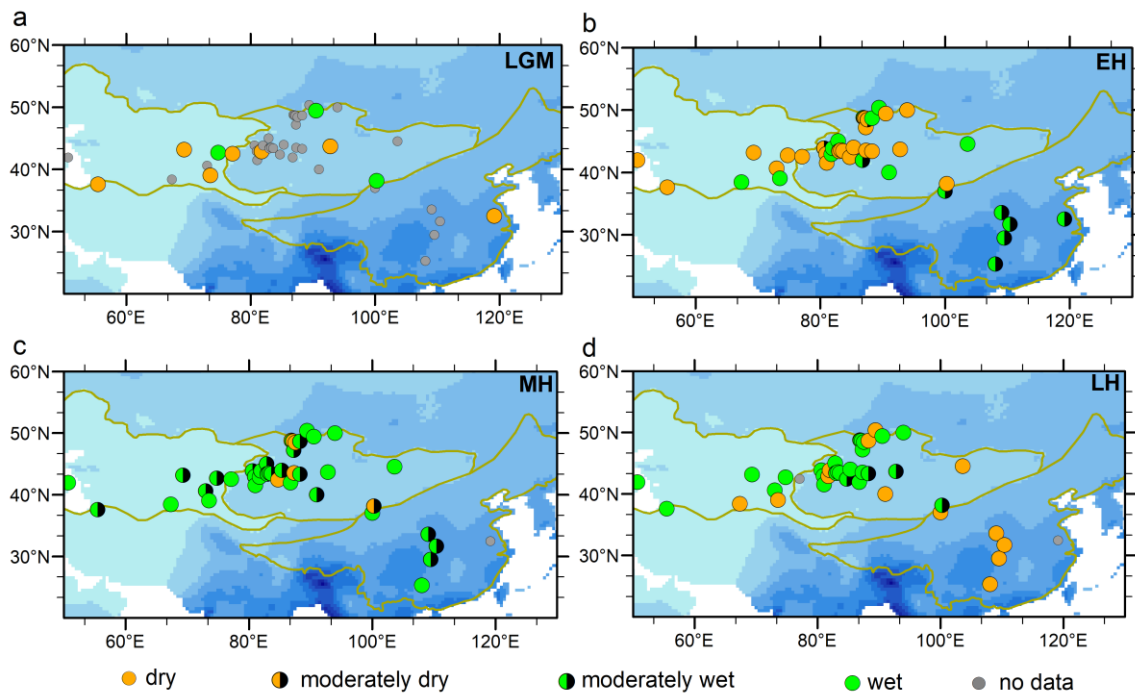
Figure 4. Spatio-temporal characteristics of the dry/wet status from 42 records since the LGM, based on the confirmation of original investigators during the LGM, early Holocene (EH), mid Holocene (MH), and late Holocene (LH). Records with an incomplete stage are shown by a gray dot. Four summarized levels of dry/wet status: wet, moderately wet, moderately dry, and dry.

In detail, we further performed a comparative analysis of the time series of typically proxy records in EA and CA (Fig. 5). The reconstructed precipitation covering the past 22,600 years from Achit Nuur suggests the wet periods from 22,600 to 13,200 cal BP (Fig. 5c). Pollen record from the Caspian Sea, controlled by the westerlies, displays that the terrestrial vegetation

around the Caspian Sea changed from desert/desert steppe during the last glacial to dry shrubland/forest during the Holocene,

210 revealing the continuous wetting process since the EH and the wettest LH (Fig. 5a). Meanwhile, results of climatically-sensitive

magnetic properties from the Xinjiang loess demonstrate that the relatively wet conditions are generally formed after ~6,000

cal BP, with the wettest climate occurring during the LH (Fig. 5b). However, there is still partially contradictory for dry/wet

status at long-term timescales in the east of CA, which are different from core regions of CA but similar to EA. Herzschuh.

(2006) comprehensively analyzed 75 paleoclimatic records in CA and revealed that wet conditions occurred during the EH

215 and MH, while the LGM was characterized by the dry climate (Fig. 5h), indicating the similarity with the monsoon climate

represented by the speleothem $\delta^{18}O$ records from Dongge Cave and Hulu Cave (Fig. 5d). High precipitation in the EH and

MH, indicated by $\delta^{18}O$ records of ostracod shells from Qinghai Lake, shows that the climate in Qinghai Lake since the late

glacial reflects the monsoon-dominated characteristic (Fig. 5e). The climate in Ulaan Nuur is wettest during the EH, humid

during the MH and dry in the LH, embodying a typical characteristic of the East Asian summer monsoon (Fig. 5f). Based on

220 the sediment cores from Lake Karakul and Lake Issyk-Kul, the EH and MH is characterized by wetter conditions in the region,

and the lake level remained low during the LGM (Fig. 5g and j). Furthermore, the regional climate in western China, inferred

from the speleothem oxygen-carbon isotope in Kesang Cave, suggests a close coupling with the Asian summer monsoon (Fig.

5i). The lake level and climate reconstructed results also showed that the "dry-cold" pattern triggered a substantial lowering

of lake level in most of arid western China, challenging the traditional view of "wet-cold" pattern and high lake levels during

225 the LGM (Zhao et al., 2015).
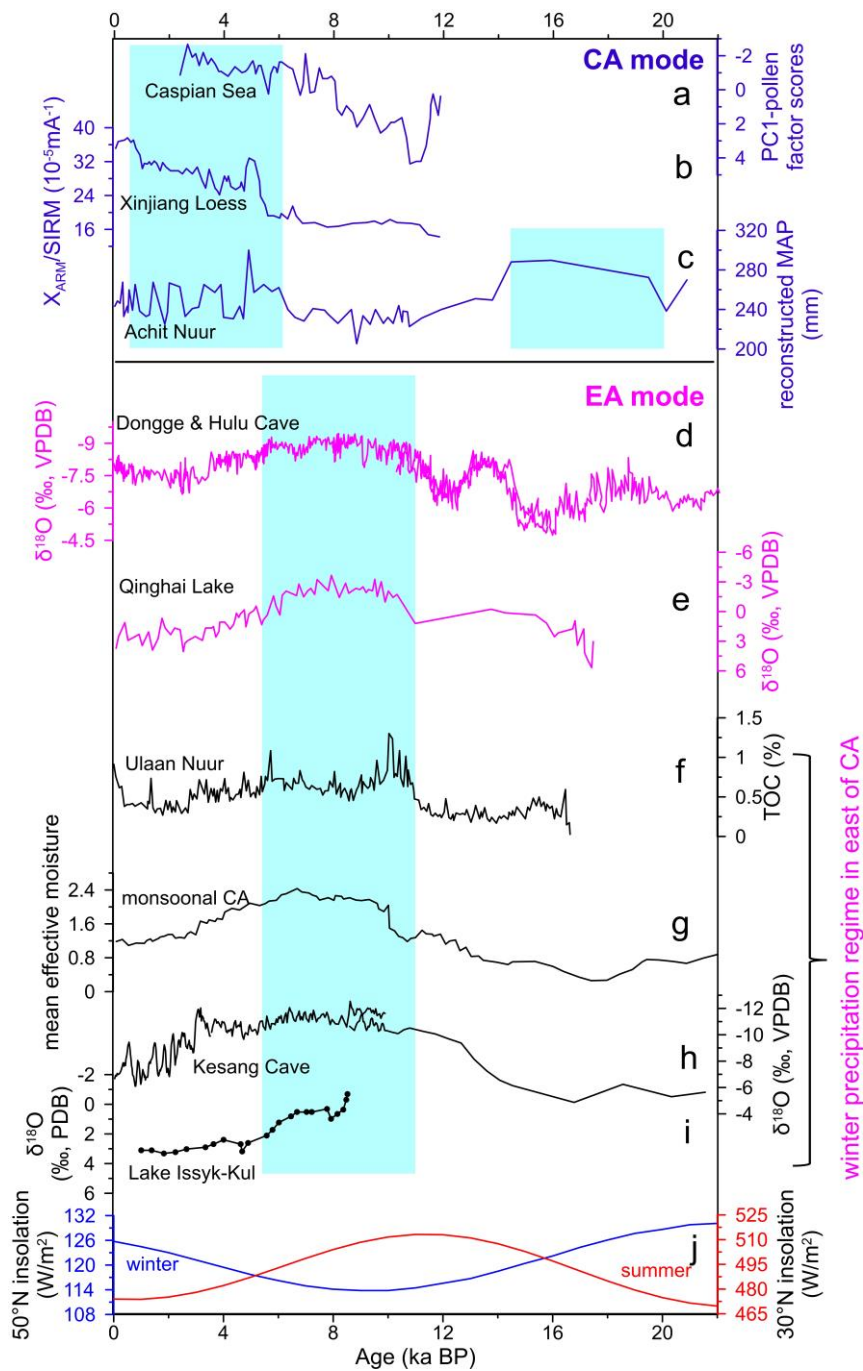
Figure 5. A comparison of proxy variability recorded in EA and CA. a Pollen record from the Caspian Sea (Leroy et al., 2014); b X_{ARM}/SIRM in the LJW10 section of the Xinjiang Loess (Chen et al., 2016); c Reconstructed MAP (mean annual precipitation) from Achit Nuur (Sun et al., 2013); d speleothem $\delta^{18}O$ values records from Dongge Cave and Hulu Cave (Yuan et al., 2004; Wang et al., 2001); e $\delta^{18}O$ of ostracode shells from Qinghai Lake (Liu et al., 2007); f TOC (Total organic carbon) from Ulaan Nuur (Lee et al., 2013); g Mean effective moisture from monsoonal Central Asia (Herzschuh, 2006); h $\delta^{18}O$ from Kesang Cave (Cheng et al., 2016); i $\delta^{18}O$ from Lake Issyk-Kul (Ricketts et al., 2001); j Summer (red line) insolation at 30°N and winter (blue line) insolation at 50°N (Berger, 1978). Blue shadows indicate the wet period of paleoclimate proxies.

4 Discussion

4.1 Possible dynamics of seasonal signals at short-term timescales

EOF analysis of precipitation and water vapor consistently verifies that the connection between EA and the east of CA exists

11

under the traditional differentiation between EA and the core region of CA. Considering that the east of CA is present as the summer precipitation regime. Therefore, we propose that seasonal signals of precipitation contribute to the connection between EA and the east of CA.
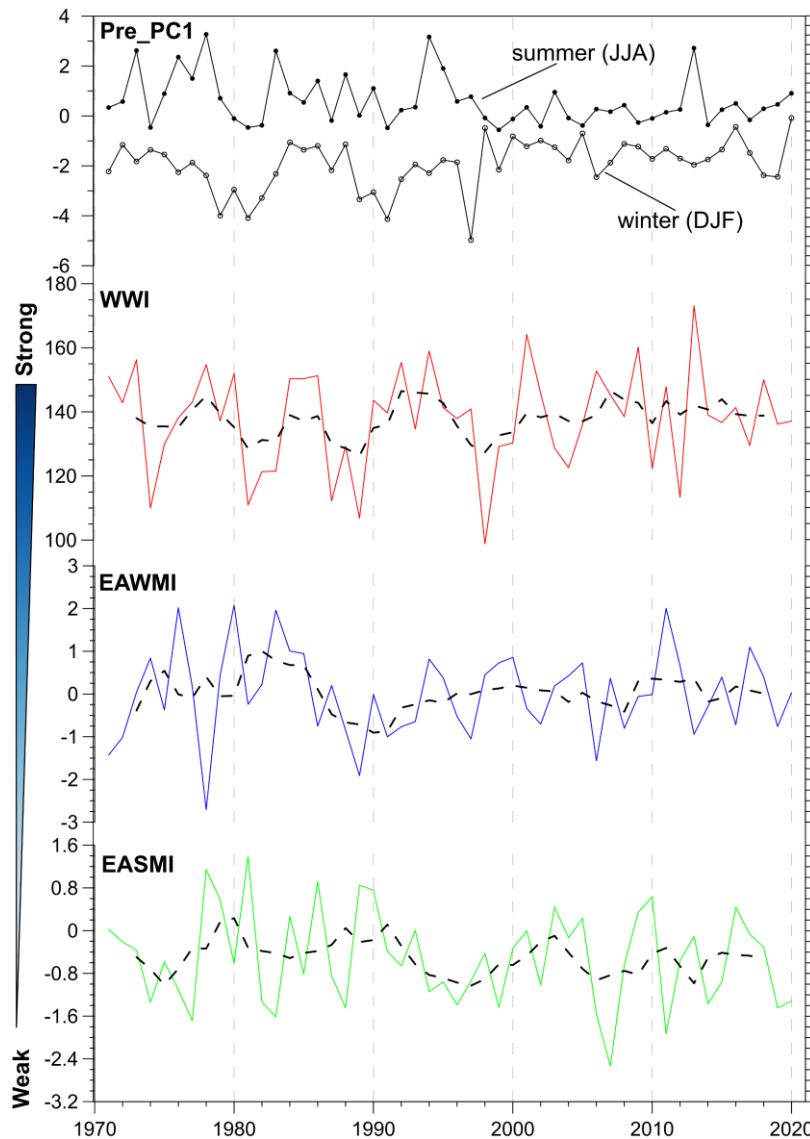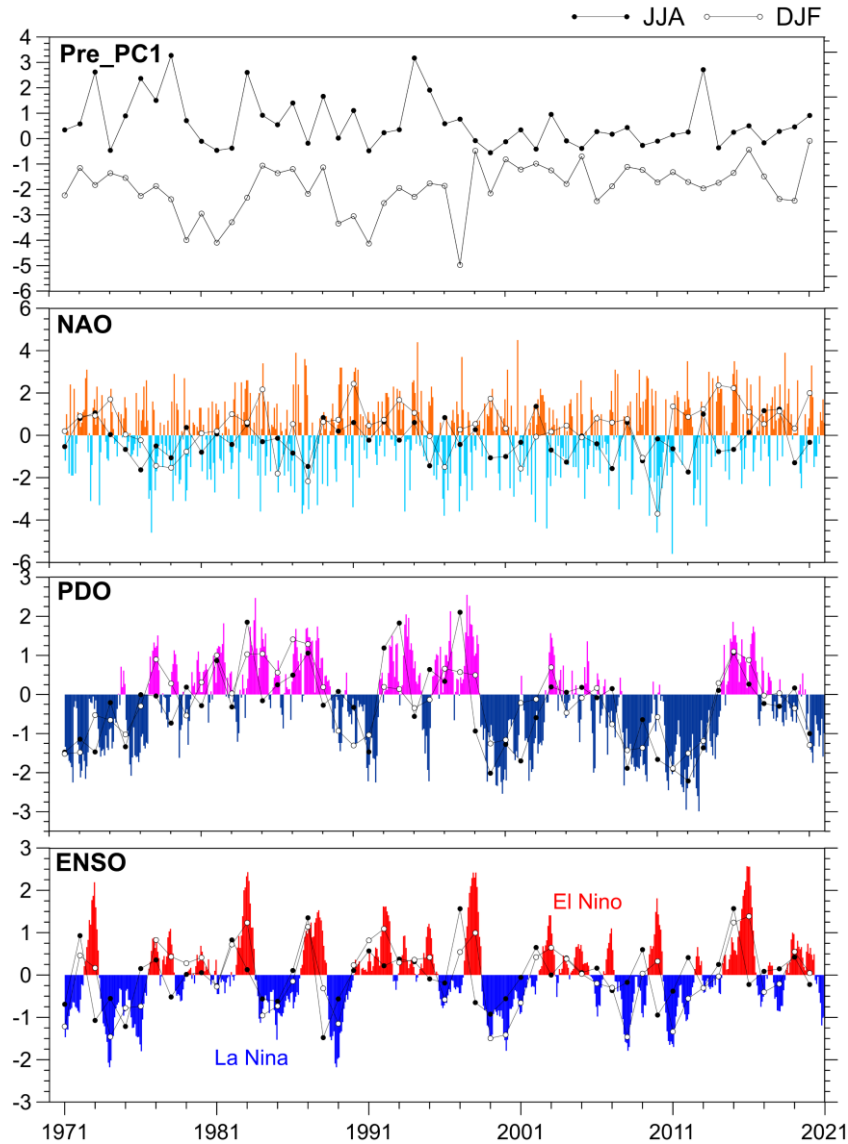

Figure 6. The time series of the precipitation PC1 in summer, winter, WWI, EAWMI, and EASMI over 1971-2020.

Generally, atmosphere circulations have important effects on the spatial distribution and the transportation of water vapor. In order to explore the influence of the modern air-sea circulation system on the summer and winter precipitation, we analyzed the time series of the precipitation PC1, WWI, EAWMI, EASMI, NAO, PDO, and ENSO over 1971 to 2020 (Fig. 6 and 7). Comparing the winter precipitation PC1 with WWI and EAWMI (Fig. 6), the weakening of the westerlies and winter monsoons is usually accompanied by an increase in winter precipitation. However, there is not a significant relationship between PC1 of summer precipitation and EASMI. As shown in Figure. 7, summer PDO and ENSO are basically similar to winter PDO and ENSO. However, the markable discrepancy exists in the evolution of winter NAO and summer NAO. The NAO and ENSO index presents interannual timescale variation, and the PDO index has an interdecadal timescale cycle. The NAO index and the winter precipitation PC1 have a positive correlation, suggesting that the North Atlantic may have certain effects on the

winter precipitation through the air-sea interaction. Positive values of the NAO index are usually accompanied by stronger midlatitude westerlies and increased water vapor content from the North Atlantic. The PDO and ENSO, however, were related to the summer precipitation PC1. The development of winter precipitation at interdecadal timescales was not connected with PDO, whereas there is a positive correlation before the 2000s between summer precipitation and PDO.


Figure 7. The time series of the precipitation PC1 in summer, winter, and annual mean, NAO, PDO, and ENSO over 1971-2020.

A majority of relevant studies stand for that precipitation variations in CA are subjected to water vapor transported by the mid-latitude westerlies, where the monsoonal water vapor source is hard to reach (Huang et al., 2015a; Guan et al., 2019). Abundant moisture is brought to CA from polar airmass, North Atlantic and the eastern Mediterranean Sea, and continues to diffuse eastward to the arid region of northwest China (Lioubimtseva, 2014). Meanwhile, several studies in recent years found that the anti-phase pattern between the East Asian summer monsoon and the westerlies causes the seesaw phenomenon of precipitation variation in northwest China (the east of CA in this study) (Zhang et al., 2019; Wu et al., 2019). However, Chen et al. (2021a) proposed that the East Asian summer monsoon plays an important role in the interdecadal variability of summer precipitation in CA through the transportation of summer water vapor from the Indian and Pacific Oceans to the east of CA.

13

265   Additionally, Huang et al. (2015b) stated that increased summer precipitation in the Tarim Basin which belongs to the east of CA is mainly related to the weakened Indian summer monsoon. In addition, the large-scale topography, such as the Qinghai-Tibet Plateau, causes the westerlies to flow around the plateau rather than over it, which in turn influences the local transport of water vapor and results in local precipitation changes (Xie et al., 2014). Therefore, the atmospheric circulation and topographic factors bear on the transportation and content of water vapor at short-term timescales, which makes the east of CA

270   with summer precipitation regime different from the core region of CA, but linked to the EA.

4.2 Possible dynamics of seasonal signals at long-term timescales

Model simulations are a valid means to visually study the mechanism of paleoclimate change in EA and CA during the LGM and MH. The results of paleoclimate simulations explain the differences and similarities in the dry/wet status from EA and CA under the framework of seasonal signals at long-term timescales. During the LGM, lower summer insolation increases the

275   meridional temperature difference and sea level pressure in the summer largely (Fig. 5k; 8a and c), leading to the strengthening of the westerlies (Fig. 9a) and further increasing precipitation in CA (Fig. 8e). Given the weakening of the LGM summer monsoon and the complex control factors (Fig. 9c), however, the summer precipitation in EA is weaker than that of MH (Fig. 8e), which is consistent with the dry/wet status reconstructed by paleoclimate records in EA (Fig. 5). Besides, although the westerlies weaken in the LGM winter (Fig. 9b), the higher winter insolation contributes to the general warming in CA and EA

280   (Fig. 5k; 8b), resulting in lower relative humidity (Fig. 8d). According to climatological theory (Barry and Richard, 2009), the decrease in relative humidity means the increase in saturated water vapor pressure, which ultimately leads to the increasing precipitation (Fig. 8f). Therefore, this elaborates the asynchrony of the long-term dry/wet status in EA and CA under the control of seasonal signals.
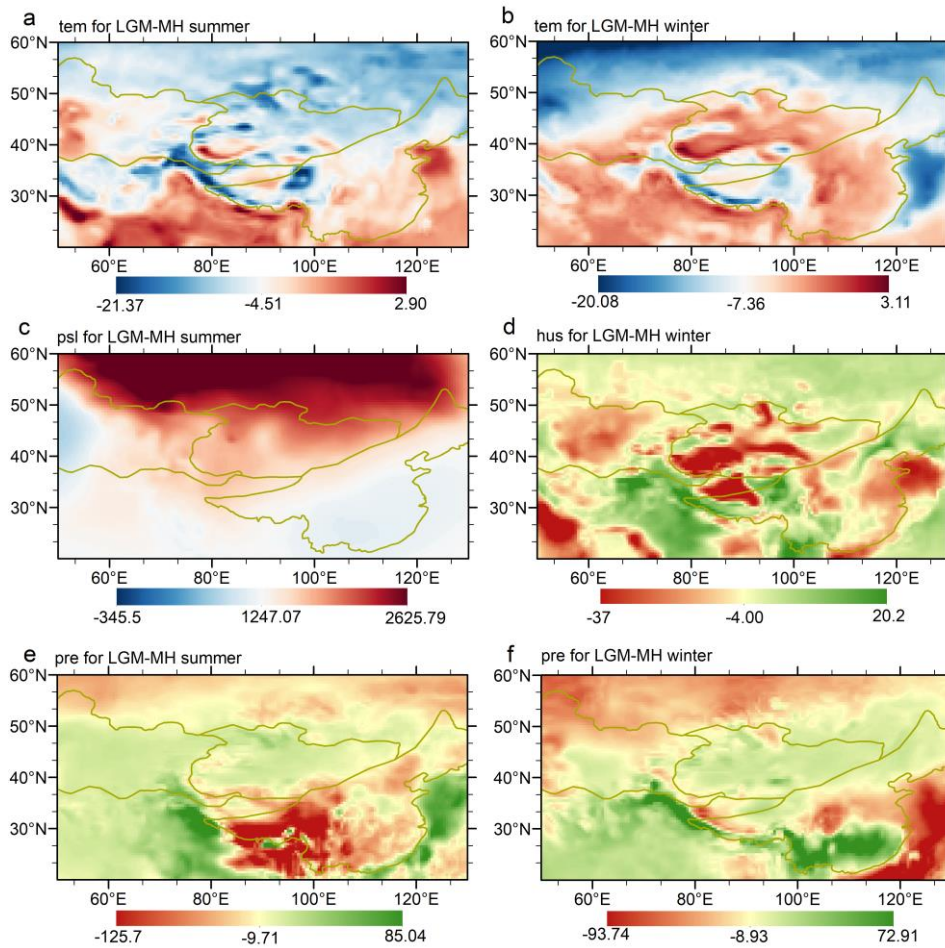
Figure 8. Summer differences of temperature (tem) (a), sea level pressure (psl) (c), and precipitation (pre) (e) for LGM-MH; and winter differences of temperature (b), relatively humid (hus) (d), and precipitation (f) for LGM-MH in EA and CA based on the PMIP3-CMIP5 multi-model ensemble.

Investigating the past climate is key to informing future climate change (Tierney et al., 2020). From the perspective of paleoclimatology, monsoon and westerlies vary greatly between LGM and MH, modulated by primary forces such as orbital insolation, greenhouse gas, and ice sheets (Oster et al., 2015; Bereiter et al., 2015; Sime et al., 2016). Paleoclimate records indicate the wet status during the LGM and LH in CA and the MH wet in EA (Fig. 5). Specifically, the dry/wet status in CA, affected by the westerlies and characterized by wet climate conditions during the LGM and mid- and late-Holocene, is opposite to that in monsoon-dominated EA. However, the proxy records in CA similar to the monsoon evolution are located in the modern summer precipitation region. From the perspective of precipitation seasonality, there are two different precipitation regimes within CA. The core region of CA has a Mediterranean climate (winter precipitation regime), with a dry summer and seasonal precipitation from early winter to late spring (Fig. 1); whereas, in the east of CA, including northwest of China and west and south of Mongolia, the summer precipitation contributes more (summer precipitation regime; Fig. 1). Therefore, summer precipitation regime may be a potential forcing factor for the linkage of paleoclimate reconstruction between EA and the east of CA, and the difference in precipitation regime may result in a divergent moisture history in EA and the core region of CA.
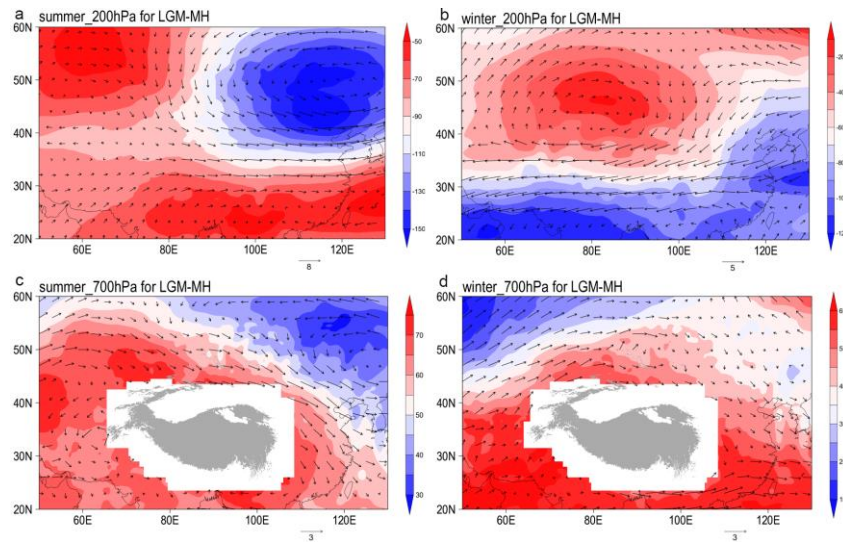
Figure 9. Summer differences of 200 hPa wind field (a) and 700 hPa wind field (c) for LGM-MH; and winter differences of 200 hPa wind field (b) and 700 hPa wind field (d) for LGM-MH in EA and CA based on the PMIP3-CMIP5 multi-model ensemble.

As a whole, our results provide a hypothesis that seasonal signals of precipitation derived from the simultaneity of rain and heat periods govern the difference and linkage in dry/wet status from EA and CA at multi-time scales. With global warming and continued increase in winter solar radiation, we suggest that the core region of CA could face a persistent reduction in precipitation in the future. Meanwhile, the decrease in summer solar radiation could lead to a strengthening and southward shift of the summer westerly jet stream over CA, potentially increasing precipitation in the east of CA with summer precipitation regimes. However, more quantitative analyses are required to understand how future interannual variations in atmospheric and oceanic circulation might control the seasonal precipitation signals that influence dry/wet status in the east of CA. Some recent work also points out increasing summer precipitation in arid CA (Chen et al., 2021a; Ren et al., 2022). Meanwhile, the phenomenon of warmer and wetter climates coincides with the simultaneity of rain and heat periods (Hu and Han, 2022). Future work should focus on the fusion of multiple datasets and high-precision climate simulation designed to evaluate the mechanism.

5 Conclusion

The summer precipitation regime in EA and the east of CA and the winter precipitation regime in the core region of CA reveal seasonal signals of precipitation. Using the EOF method, this study analyzes the spatiotemporal variations of precipitation in EA and CA. Results reveal that seasonal signals derived from the simultaneity of rain and heat periods are important factors linking climate change modes in EA and CA at short-term timescales. A compilation of 42 proxy records with reliable chronologies enables us to reassess the dry/wet status in EA and CA since the LGM. In core regions of CA, dry/wet status is usually characterized by dry EH and wet LH. However, part of records in the east of CA with simultaneous rain and heat periods hold the same dry/wet status with EA, i.e., the dry condition during the LGM and the wet climate during the EH and MH. This also reflects another meaning of seasonal signals at long-term timescales, namely the "dry-cold" pattern and "wet-

16

warm" pattern. Concurrently, paleoclimate records reflect seasonal signals triggered by the insolation at long-term timescales.

325 The multi-model ensemble simulations of multiple climatic elements explain the climate mechanism of differences and linkage in dry/wet status from EA and CA since the LGM. Results show that summer insolation influences the meridional temperature gradient and sea level pressure in the summer, changing the intensity of the westerly winds and summer monsoon and further controlling the summer precipitation in EA and the east of CA. Meanwhile, winter insolation contributes to the general warming in EA and the core region of CA, and in turn results in lower relative humidity, which ultimately increases winter

330 precipitation during the LGM.

In general, the seasonal signals of precipitation derived from the simultaneity and non-simultaneity of rain and heat periods on short-term timescales can also affect the dry/wet status on long-term timescales, but their influencing factors are different. Due to the influence of precipitation seasonal signals on multi-time scales, CA with the winter precipitation regime and EA with the summer precipitation regime show traditional anti-phase in the evolution of dry/wet status. However, it is worth noting

335 that in the east of CA with simultaneous rain and heat, there is the same dry/wet evolution as in EA. Therefore, we believe that seasonal signals can provide important insight for analyzing the differences and linkages in climate change between CA and EA on multi-time scales.

340

345

350

355

Author contributions. YL initiated the work. YL and SP conceived the manuscript. SP finished the data sorting, statistical and geospatial data analysis, visualizations of the work, the original draft preparation, and editing and revising of this manuscript. ZZ, MG, XC, JD, YX revised the manuscript.

References

An, C., Feng, Z., Barton, L.: 2006. Dry or humid? Mid-Holocene humidity changes in arid and semi-arid China, Quat. Sci. Rev., 25, 351-61, https://doi.org/10.1016/j.quascirev.2005.03.013, 2006.

An, C., Lu, Y., Zhao, J., Tao, S., Dong, W., Li, H., Jin, M., Wang, Z.: A high-resolution record of Holocene environmental and climatic changes from Lake Balikun (Xinjiang, China): implications for central Asia, Holocene, 22, 43-52, https://doi.org/10.1177/0959683611405244, 2012.

Barichivich, J., Osborn, T. J., Harris, I., van der Schrier, G., Jones, P. D. Monitoring global drought using the self-calibrating Palmer Drought Severity Index [in "State of the Climate in 2020"], B. Am. Meteorol. Soc., 101, S51-S52, 2021.

Barry, R. G. and Richard, J. C.: Atmosphere, weather and climate, Routledge, https://doi.org/10.4324/9780203871027, 2009.

Bereiter, B., Eggleston, S., Schmitt, J., Nehrbass-Ahles, C., Stocker, T. F., Fischer, H., Kipfstuhl, S., Chappellaz, J.: Revision of the EPICA Dome C CO_2 record from 800 to 600 kyr before present, Geophys. Res. Lett., 42, 542-549, https://doi.org/10.1002/2014GL061957, 2015.

Blyakharchuk, T. A., Wright, H. E., Borodavko, P. S., van der Knaap, W. O., Ammann, B.: Late glacial and Holocene

vegetational history of the Altai mountains (southwestern tuva republic, siberia), Palaeogeogr. Palaeoclimatol. Palaeoecol., 245, 518-534, https://doi.org/10.1016/j.palaeo.2006.09.010, 2007.

Briegleb, B. P., Bitz, C. M., Hunke, E. C., Lioscomb, W. H., Holland, M. M., Schramm, J. L., Moritz, A. R.: Scientific description of the sea ice component in the community climate system model, Version 3, 70, https://doi.org/10.5065/D6HH6H1P, 2004.

Cai, Y., Tan, L., Cheng, H., An, Z., Edwards, R. L., Kelly, M. M., Kong, X., Wang, X.: The variation of summer monsoon precipitation in central China since the last deglaciation, Earth Planet. Sci. Lett., 291, 21-31, https://doi.org/10.1016/j.epsl.2009.12.039, 2010.

Chen, C., Zhang, X., Lu, H., Jin, L., Du, Y., Chen, F.: Increasing summer precipitation in arid central Asia linked to the weakening of the East Asian summer monsoon in the recent decades, Int. J. Climatol., 41, 1024-1038, https://doi.org/10.1002/joc.6727, 2021a.

Chen, F., Yu, Z., Yang, M., Ito, E., Wang, S., David, B. M., Huang, X., Zhao, Y., Sato, T., Birks, H. J. B., Boomer, I., Chen, J., An, C., Wünnemann, B.: Holocene moisture evolution in arid Central Asia and its out-of-phase relationship with Asian monsoon history, Quat. Sci. Rev., 27, 351-364, https://doi.org/10.1016/j.quascirev.2007.10.017, 2008.

Chen, F., Chen, J., Huang, W.: A discussion on the westerly-dominated climate model in mid-latitude Asia during the modern interglacial period, Earth Sci. Front., 16, 23-32, 2009. (in Chinese with English abstract)

Chen, F., Xu, Q., Chen, J., Birks, H. J. B., Liu, J., Zhang, S., Jin, L., An, C., Telford, R. J., Cao, X., Wang, Z., Zahng, X., Selvaraj, K., Lü, H., Li, Y., Zheng, Z., Wang, H., Zhou, A., Dong, G., Zhang, J., Huang, X., Bloemendal, J., Rao, Z.: East Asian summer monsoon precipitation variability since the last deglaciation, Sci. Rep., 5, 11186, https://doi.org/10.1038/srep11186, 2015.

Chen, F., Jia, J., Chen, J., Li, G., Zhang, X., Xie, H., Xia, D., Huang, W., An, C.: A persistent Holocene wetting trend in arid central Asia, with wettest conditions in the late Holocene, revealed by multi-proxy analyses of loess-paleosol sequences in Xinjiang, China, Quat. Sci. Rev., 146, 134-146, https://doi.org/10.1016/j.quascirev.2016.06.002, 2016.

Chen, G. and Huang, R.: Excitation mechanisms of the tele-connection patterns affecting the July precipitation in North-west China, J. Clim., 25, 7834-7851, 2012.

Chen, F., Chen, J., Huang, W., Chen, S., Huang, X., Jin, L., Jia, J., Zhang, X., An, C., Zhang, J., Zhao, Y.: Westerlies Asia and monsoonal Asia: spatiotemporal differences in climate change and possible mechanisms on decadal to suborbital timescales, Earth Sci. Rev., 192, 337-354, https://doi.org/10.1016/j.earscirev.2019.03.005, 2019.

Chen, F., Chen, J., Huang, W.: Weakened East Asian summer monsoon triggers increased precipitation in Northwest China, Sci. China Earth Sci., 64, 835-837, https://doi.org/10.1007/s11430-020-9731-7, 2021b.

Chen, S., Liu, J., Wang, X., Zhao, S., Chen, J., Qiang, M., Liu, B., Xu, Q., Xia, D., Chen, F.: Holocene dust storm variations over northern China: transition from a natural forcing to an anthropogenic forcing, Sci. Bull., 66, 2516-2527,

https://doi.org/10.1016/j.scib.2021.08.008, 2021c.

415   Chen, S., Chen, J., Lv, F., Liu, X., Huang, W., Wang, T., Liu, J., Hou, J., Chen, F.: Holocene moisture variations in arid central Asia: Reassessment and reconciliation, Quat. Sci. Rev., 297, 107821, https://doi.org/10.1016/j.quascirev.2022.107821, 2022.

Cheng, H., Zhang, P., Spötl, C., Edwards, R. L., Cai, Y., Zhang, D., Sang, W., Tan, M., An, Z.: The climatic cyclicity in semiarid-arid central Asia over the past 500,000 years, Geophys. Res. Lett., 39, L01705,

420   https://doi.org/10.1029/2011gl050202, 2012.

Cheng, H., Spötl, C., Breitenbach, S. F. M., Sinha, A., Wassenburg, J. A., Jochum, K. P., Scholz, D., Li, X., Peng, Y., Lv, Y., Zhang, P., Votintseva, A., Loginov, V., Ning, Y. F., Kathayat, G., Edwards, R. L.: Climate variations of Central Asia on orbital to millennial timescales, Sci. Rep., 6, 36975, Climate variations of Central Asia on orbital to millennial timescales, 2016.

425   Dykoski, C. A., Edwards, R. L., Cheng, H., Yuan, D., Cai, Y., Zhang, M., Lin, Y., Qing, J., An, Z., Revenaugh, J.: A high-resolution, absolute-dated Holocene and deglacial Asian monsoon record from Dongge Cave, China, Earth Planet. Sci. Lett., 233, 71-86, https://doi.org/10.1016/j.epsl.2005.01.036, 2005.

Feng, Z., Sun, A., Abdusalih, N., Ran, M., Kurban, A., Lan, B., Zhang, D., Yang, Y.: Vegetation changes and associated climatic changes in the southern Altai Mountains within China during the Holocene, Holocene, 27, 683-693,

430   https://doi.org/10.1177/0959683616670469, 2016.

Gao, F., Jia, J., Xia, D., Lu, C., Lu, H., Wang, Y., Liu, H., Ma, Y., Li, K.: Asynchronous Holocene climate optimum across mid-latitude Asia, Palaeogeogr. Palaeoclimatol. Palaeoecol., 518, 206e214, https://doi.org/10.1016/j.palaeo.2019.01.012, 2019.

Gent, P. R., Danabasoglu, G., Donner, L. J., Holland, M. M., Hunke, E. C., Jayne, S. R., Lawrence, D. M., Neale, R. B., Rasch,

435   P. J., Vertenstein, M.: The community climate system model version 4, J. Clim., 24, 4973-4991, https://doi.org/10.1175/2011jcli4083.1, 2011.

Guan, X., Yang, L., Zhang, Y., Li, J.: Spatial distribution, temporal variation, and transport characteristics of atmospheric water vapor over Central Asia and the arid region of China, Global Planet. Change, 172, 159-178, https://doi.org/10.1016/j.gloplacha.2018.06.007, 2019.

440   Han, S., Wu, N., Li, Z.: Inland climate changes in Dzungaria during the late Pleistocene Epoch, Geog. Res., 12, 47-54, 1993. (in Chinese with English abstract).

Han, S. and Qu, Z.: Inland Holocene climatic features recorded in Balikun lake, northern Xinjiang. Science in China Series B-Chemistry, Life Sciences & Earth Sciences, 11, 1201-1209, 1992. (in Chinese with English abstract)

Harris, I., Jones, P. D., Osborn, T. J., Lister, D. H.: Updated high-resolution grids of monthly climatic observations-the CRU

445   TS3.10 Dataset, Int. J. Climatol., 34, 623-642, 2014.

Heinecke, L., Mischke, S., Adler, K., Barth, A., Biskaborn, B. K., Plessen, B., Ingmar, N., Gerhard, K., Ilhomjon, R., Herzschuh, U.: Climatic and limnological changes at Lake Karakul (Tajikistan) during the last ~29 cal ka, J. Paleolimnol., 58, 317-334, https://doi.org/10.1007/s10933-017-9980-0, 2017.

Hersbach, H., Bell, B., Berrisford, P., Hirahara, S., Horányi, A., Muñoz-Sabater, J., Nicolas, J., Peubey, C., Radu, R., Schepers, D., Simmons, A., Soci, C., Abdalla, S., Abellan, X., Balsamo, G., Bechtold, P., Biavati, G., Bidlot, J., Bonavita, M., De Chiara, G., Dahlgren, P., Dee, D., Diamantakis, M., Dragani, R., Flemming, J., Forbes, R., Fuentes, M., Geer, A., Haimberger, L., Healy, S., Hogan, J. R., Holm, E., Janiskova, M., Keeley, S., Laloyaux, P., Lopez, P., Lupu, C., Radnoti, G., de Rosnay, P., Rozum, I., Vamborg, F., Villaume, S., Thepaut, J.: The ERA5 global reanalysis, Q. J. Roy. Meteor. Soc., 146, 1999-2049, https://doi.org/10.1002/qj.3803, 2020.

Herzschuh, U.: Palaeo-moisture evolution in monsoonal central Asia during the last 50,000 years, Quat. Sci. Rev., 25, 163-178, https://doi.org/10.1016/j.quascirev.2005.02.006, 2006.

Hu, Q. and Han, Z.: Northward Expansion of Desert Climate in Central Asia in Recent Decades, Geophys. Res. Lett., 49, e2022GL098895, https://doi.org/10.1029/2022gl098895, 2022.

Huang, W., Chen, J., Zhang, X., Feng, S., Chen, F.: Definition of the core zone of the "westerlies-dominated climatic regime", and its controlling factors during the instrumental period, Sci. China Earth Sci., 58, 676-684, https://doi.org/10.1007/s11430-015-5057-y, 2015a.

Huang, W., Feng, S., Chen, J., Chen, F.: Physical mechanisms of summer precipitation variations in the Tarim basin in northwestern China, J. Clim., 28, 3579-3591, https://doi.org/10.1175/jcli-d-14-00395.1, 2015b.

Huang, X., Chen, F., Fan, Y., Yang, M.: Dry late-glacial and early Holocene climate in arid central Asia indicated by lithological and palynological evidence from Bosten Lake, China. Quat. Int., 194, 19-27, https://doi.org/10.1016/j.quaint.2007.10.002, 2009.

Hurrell, J. W. and Deser, C.: North Atlantic climate variability: The role of the North Atlantic Oscillation, J. Mar. Syst., 78, 28-41, https://doi.org/10.1016/j.jmarsys.2008.11.026, 2009.

Hurrell, J. W.: Decadal Trends in the North Atlantic Oscillation: Regional Temperatures and Precipitation, Science, 269, 676-679, https://doi.org/10.1126/science.269.5224.676, 1995.

Jia, J., Chen, J., Wang, Z., Chen, S., Wang, Q., Wang, L., Yang, L., Xia, D., Chen, F.: No evidence for an anti-phased Holocene moisture regime in mountains and basins in Central Asian: records from Ili loess, Xinjiang, Palaeogeogr. Palaeoclimatol. Palaeoecol., 572, 110407, https://doi.org/10.1016/j.palaeo.2021.110407, 2021.

Jiang, Q., Ji, J., Shen, J., Matsumoto, R., Tong, G., Qian, P., Ren, X., Yan, D.: Holocene vegetational and climatic variation in westerly-dominated areas of Central Asia infrred from the Sayram Lake in northern Xinjiang, China, Sci. China Earth Sci., 56, 339-353, https://doi.org/10.1007/s11430-012-4550-9, 2013.

Jiang, Q., Meng, B., Wang, Z., Qian, P., Zheng, J., Jiang, J., Zhao, C., Hou, J., Dong, G., Shen, J., Liu, W., Liu, Z., Chen, F.:

Exceptional terrestrial warmth around 4200-2800 years ago in Northwest China, Sci. Bull., 67, 427-436, https://doi.org/10.1016/j.scib.2021.11.001, 2022.

480 Joussaume, S., Taylor, K. E., Braconnot, P. J. F. B., Mitchell, J. F. B., Kutzbach, J. E., Harrison, S. P., Prentice, I. C., Broccoli, A. J., Abe-Ouchi, A., Bartlein, P. J., Bonfils, C.: Monsoon changes for 6000 years ago: results of 18 simulations from the paleoclimate modeling intercomparison project (PMIP), Geophys. Res. Lett., 26, 859-862, https://doi.org/10.1029/1999gl900126, 1999.

Kang, S., Wang, X., Roberts, H. M., Duller, G. A., Song, Y., Liu, W., Zhang, R., Liu, X., Lan, J.: Increasing effective moisture

485 during the Holocene in the semiarid regions of the Yili Basin, central Asia: evidence from loess sections, Quat. Sci. Rev., 246, 106553, https://doi.org/10.1016/j.quascirev.2020.106553, 2020.

Lee, M. K., Lee, Y. I., Lim, H. S., Lee, J. I., Yoon, H. I.: Late Pleistocene-H olocene records from Lake Ulaan, southern Mongolia: implications for east Asian palaeomonsoonal climate changes, J. Quat. Sci., 28, 370-378, https://doi.org/10.1002/jqs.2626, 2013.

490 Leroy, S. A., López-Merino, L., Tudryn, A., Chalié, F., Gasse, F.: Late Pleistocene and Holocene palaeoenvironments in and around the middle Caspian basin as reconstructed from a deep-sea core, Quat. Sci. Rev., 101, 91-110, https://doi.org/10.1016/j.quascirev.2014.07.011, 2014.

Leroy, S. A. G., Ricketts, R. D., Rasmussen, K. A.: Climatic and limnological changes 12,750 to 3600 years ago in the Issyk-Kul catchment, Tien Shan, based on palynology and stable isotopes, Quat. Sci. Rev., 259, 106897,

495 https://doi.org/10.1016/j.quascirev.2021.106897, 2021.

Leroy, S. A. G., Lopez-Merino, L., Tudryn, A., Chalie, F., Gasse, F.: Late Pleistocene and Holocene palaeoenvironments in and around the middle Caspian basin as reconstructed from a deep-sea core, Quat. Sci. Rev., 101, 91-110, https://doi.org/10.1016/j.quascirev.2014.07.011 2014.

Li, J.: The patterns of environmental changes since last Pleistoc ene in northwestern China, Quat. Sci., 3, 197-204, 1990. (in

500 Chinese with English abstract)

Li, X., Zhao, K., Dodson, J., Zhou, X.: Moisture dynamics in central Asia for the last 15 kyr: new evidence from Yili Valley, Xinjiang, NW China, Quat. Sci. Rev., 30, 3457-3466, https://doi.org/10.1016/j.quascirev.2011.09.010, 2011.

Li, Y., Song, Y., Kaskaoutis, D. G., Zan, J., Orozbaev, R., Tan, L., Chen, X.: Aeolian dust dynamics in the Fergana Valley, Central Asia, since~30 ka inferred from loess deposits, Geosci. Front., 12, 101180,

505 https://doi.org/10.1016/j.gsf.2021.101180, 2021.

Li, Y., Song, Y., Orozbaev, R., Dong, J., Li, X., Zhou, J.: Moisture evolution incentral Asia since 26 ka: insights from a Kyrgyz loess section, western tian Shan, Quat. Sci. Rev. 249, 106604, https://doi.org/10.1016/j.quascirev.2020.106604, 2020a.

Li, Y., Peng, S., Liu, H., Zhang, X., Ye, W., Han, Q., Zhang, Y., Xu, L., Li, Y.: Westerly jet stream controlled climate change mode since the Last Glacial Maximum in the northern Qinghai-Tibet Plateau, Earth Planet. Sci. Lett., 549, 116529,

510   https://doi.org/10.1016/j.epsl.2020.116529, 2020b.

Lioubimtseva, E.: Impact of Climate Change on the Aral Sea and its Basin. The Devastation and Partial Rehabilitation of a
        Great Lake, The Aral Sea, 405-427, https://doi.org/10.1007/978-3-642-02356-9_17, 2014.

Liu, X., Shen, J., Wang, S., Wang, Y., Liu, W.: Southwest monsoon changes indicated by oxygen isotope of ostracode shells
        from sediments in Qinghai lake since the late glacial, Chin. Sci. Bull., 4, 109-114, https://doi.org/10.1007/s11434-007-
515   0086-3, 2007.

Liu, X., Liu, J., Shen, C., Yang, Y., Chen, J., Chen, S., Wang, X., Wu, C., Chen, F.: Inconsistency between records of $\delta^{18}O$ and
        trace element ratios from stalagmites: evidence for increasing midelate Holocene moisture in arid central Asia, Holocene,
        30, 369-379, https://doi.org/10.1177/0959683619887, 2020.

Lorenz, E.: Empirical orthogonal function and statistical weather prediction. Scientific Report No. 1 Statist Forecasting Project.
520   Department of Meteorology, Massachusetts Institute of Technology, 1956.

Manoj, M. C., Srivastava, J., Uddandam, P. R., Thakur, B.: A 2000 year multiproxy evidence of natural/anthropogenic influence
        on climate from the southwest coast of India, J. Earth Sci., 31, 1029-1044, https://doi.org/10.1007/s12583-020-1336-4,
        2020.

Mantua,   N.   J.   and   Hare,   S.   R.:   The   Pacific   Decadal   Oscillation,   J.   Oceanogr.,   58,   35-44,
525   https://doi.org/10.1023/A:1015820616384, 2002.

Mischke, S., Lai, Z., Aichner, B., Heinecke, L., Makhmudov, Z., Kuessner, M. L., Herzschuh, U.: Radiocarbon and optically
        stimulated luminescence dating of sediments from Lake Karakul, Tajikistan, Quat. Geochronol., 41, 51-61,
        https://doi.org/10.1016/j.quageo.2017.05.008, 2017.

Nagashima, K., Tada, R., Tani, A., Sun, Y., Isozaki, Y., Toyoda, S., Hasegawa, H.: Millennial-scale oscillations of the westerly
530   jet path during the last glacial period, J. Asian Earth Sci., 40, 1214-1220, https://doi.org/10.1016/j.jseaes.2010.08.010,
        2011.

Peltier, W. R.: Global glacial isostasy and the surface of the ice-age Earth: The ICE-5G (VM2) model and GRACE, Annu. Rev.
        Earth Planet. Sci., 32, 111-149, https://doi.org/10.1146/annurev.earth.32.082503.144359, 2004.

Peng, D. and Zhou, T.: Why was the arid and semiarid North-west China getting wetter in the recent decades, J. Geophys. Res.
535   Atmos., 122, 9060-9075, https://doi.org/10.1002/2016JD026424, 2017.

Ran, M. and Feng, Z.: Variation in carbon isotopic composition over the past ca. 46,000 yr in the loessepaleosol sequence in
        central   Kazakhstan   and   paleoclimatic   significance,   Org.   Geochem.,   73,   47-55,
        https://doi.org/10.1016/j.orggeochem.2014.05.006, 2014.

Randall, D. A., Wood, R. A., Bony, S., Colman, R., Taylor, K. E.: Climate models and their evaluation. In Climate change
540   2007: The physical science basis. Contribution of Working Group I to the Fourth Assessment Report of the IPCC (FAR)
        (pp. 589-662), Cambridge University Press, 2007.

Rayner, N. A. A., Parker, D. E., Horton, E. B., Folland, C. K., Alexander, L. V., Rowell, D. P., Kent, E. C.: Global analyses of sea surface temperature, sea ice, and night marine air temperature since the late nineteenth century, J. Geophys. Res. Atmos., 108, 4407, https://doi.org/10.1029/2002jd002670, 2003.

545 Ren, Y., Yu, H., Liu, C., He, Y., Huang, J., Zhang, L., Hu, H., Zhang, Q., Chen, S., Liu, X., Zhang, M., Wei, Y., Yang, Y., Fan, W., Zhou, J.: Attribution of Dry and Wet Climatic Changes over Central Asia, J. Clim., 35,1399-1421, https://doi.org/10.1175/jcli-d-21-0329.1, 2021.

Ricketts, R. D., Johnson, T. C., Brown, E. T., Rasmussen, K. A., Romanovsky, V. V.: The Holocene paleolimnology of Lake Issyk-Kul, Kyrgyzstan: trace element and stable isotope composition of ostracodes, Palaeogeogr. Palaeoclimatol.

550 Palaeoecol., 176, 207-227, https://doi.org/10.1016/s0031-0182(01)00339-x, 2001.

Rotstayn, L., Collier, M., Dix, M., Feng, Y., Gordon, H., O'Farrell, S., Smith, I., Syktus, J.: Improved simulation of Australian climate and ENSO-related climate variability in a GCM with an interactive aerosol treatment, Int. J. Climatol., 30, 1067-1088, https://doi.org/10.1002/joc.1952, 2010.

Rudaya, N., Tarasov, P., Dorofeyuk, N., Solovieva, N., Kalugin, I., Andreev, A., Daryin, A., Diekmann, B., Riedel, F.,

555 Tserendash, N., Wagner, M.: Holocene environments and climate in the Mongolian Altai reconstructed from the Hoton-Nur pollen and diatom records: a step towards better understanding climate dynamics in Central Asia, Quat. Sci. Rev., 28, 540-554, https://doi.org/10.1016/j.quascirev.2008.10.013, 2009.

Schmidt, G. A., M. Kelley, L. Nazarenko, R. Ruedy, G. L. Russell, I. Aleinov, M. Bauer, S. E. Bauer, M. K. Bhat, R. Bleck, V. Canuto, Y. Chen, Y. Cheng, T. L. Clune, A. Del Genio, R. de Fainchtein, G. Faluvegi, J. E. Hansen, R. J. Healy, N. Y.

560 Kiang, D. Koch, A. Lacis, A. N. LeGrande, J. Lerner, K. K. Lo, E. E. Matthews, S. Menon, R. L. Miller, V. Oinas, A. O. Oloso, J. P. Perlwitz, M. J. Puma, W. M. Putman, D. Rind, A. Romanou, M. Sato, D. Shindell, S. Sun, R. A. Syed, N. Tausnev, K. Tsigaridis, N. Unger, A. Voulgarakis, M. Yao, J. Zhang.: Configuration and assessment of the GISS ModelE2 contributions to the CMIP5 archive, J. Adv. Modeling Earth Syst., 6, 141-184, https://doi.org/10.1002/2013MS000265, 2014.

565 Sorg, A., Bolch, T., Stoffel, M., Solomina, O., Beniston, M.: Climate change impacts on glaciers and runoff in Tien Shan (Central Asia), Nature Clim Change, 2, 725-731, https://doi.org/10.1038/nclimate1592, 2012.

Sun, A., Feng, Z., Ran, M., Zhang, C.: Pollen-recorded bioclimatic variations of the last ~22,600 years retrieved from Achit Nuur core in the western Mongolian Plateau, Quat. Int., 311, 36-43, https://doi.org/10.1016/j.quaint.2013.07.002, 2013.

Tao, S., An, C., Chen, F., Tang, L., Wang, Z., Lü, Y., Li, Z., Zheng, T., Zhao, J.: Pollen-inferred vegetation and environmental

570 changes since 16.7 ka BP at Balikun Lake, Xinjiang, Chin. Sci. Bull., 55, 2449-2457, https://doi.org/10.1007/s11434-010-3174-8, 2010.

Tian, F., Herzschuh, U., Telford, R. J., Mischke, S., Van der Meeren, T., Krengel, M.: A modern pollen-climate calibration set from central-western Mongolia and its application to a late glacial-Holocene record, J. Biogeogr., 41, 1909-1922,

https://doi.org/10.1111/jbi.12338, 2014.

575   Tierney, J. E., Poulsen, C. J., Montañez, I. P., Bhattacharya, T., Feng, R., Ford, H. L., Hönisch, B., Inglis, G. N., Petersen, S. V., Sagoo, N., Tabor, C. R., Thirumalai, K., Zhu, J., Burls, N. J., Foster, G. L., Goddéris, Y., Huber, B. T., Ivany, L. C., Kirtland, Turner, S., Lunt, D. J., McElwain, J. C., Mills, B. J. W., Otto-Bliesner, B. L., Ridgwell, A., Zhang, Y.: Past climates inform our future, Science, 370, eaay3701, https://doi.org/10.1126/science.aay3701, 2020.

Voldoire, A., Sanchez-Gomez, E., Mélia, D. S. Y, Decharme, B., Cassou, C., Sénési, S., Valcke, S., Beau, I., Alias, A.,
580   Chevallier, M., Déqué, M., Deshayes, J., Douville, H., Fernandez, E., Madec, G., Maisonnave, E., Moine, M. P., Planton, S., Saint-Martin, D., Szopa, S., Tyteca, S., Alkama, R., Belamari, S., Braun, A., Coquart, L., Chauvin, F.: The CNRM-CM5.1 global climate model: description and basic evaluation, Clim. Dyn., 40, 2091-2121, https://doi.org/10.1007/s00382-011-1259-y, 2013.

Wang, B., Liu, J., Kim, H. J., Webster, P. J., Yim, S. Y.: Recent change of the global monsoon precipitation (1979-2008), Clim.
585   Dyn., 39, 1123-1135, https://doi.org/10.1007/s00382-011-1266-z, 2012.

Wang, L., Jia, J., Xia, D, Liu, H., Gao, F., Duan, Y., Wang, Q., Xie, H., Chen, F.: Climate change in arid central Asia since MIS 2 revealed from a loess sequence in Yili Basin, Xinjiang, China, Quat. Int., 502, 258-266, https://doi.org/10.1016/j.quaint.2018.02.032, 2018.

Wang, P., Wang, B., Cheng, H., Fasullo, J., Guo, Z., Kiefer, T., Liu, Z.: The global monsoon across time scales: Mechanisms
590   and outstanding issues, Earth Sci. Rev., 174, 84-121, https://doi.org/10.1016/j.earscirev.2017.07.006, 2017.

Wang, Y., Cheng, H., Edwards, R. L., An, Z., Wu, J., Shen, C, Dorale, J. A.: A high-resolution absolute-dated late Pleistocene monsoon record from Hulu cave, China, Science, 294, 2345-2348, https://doi.org/10.1126/science.1064618, 2001.

Wang, Q., Wei, H., Khormali, F., Wang, L., Xie, H., Wang, X., Huang, W., Chen, J., Chen, F.: Holocene moisture variations in western arid central Asia inferred from loess records from NE Iran, G-cubed, 21, e2019GC008616,
595   https://doi.org/10.1029/2019gc008616, 2020.

Watanabe, S., Hajima, T., Sudo, K., Nagashima, T., Takemura, T., Okajima, H., Nozawa, T., Kawase, H., Abe, M., Yokohata, T., Ise, T., Sato, H., Kato, E., Takata, K., Emori, S., Kawamiya, M.: MIROC-ESM 2010: model description and basic results of CMIP5-20c3m experiments, Geosci. Model Dev., 4, 845-872, https://doi.org/10.5194/gmd-4-845-2011, 2011.

Wei, W., Zhang, R., Wen, M., Yang, S.: Relationshipbetween the Asian westerly jet stream and summer rainfall over Central
600   Asia and North China: roles of the Indian mon-soon and the south Asian high, J. Clim., 30, 537-552, https://doi.org/10.1175/JCLI-D-15-0814.1, 2017.

Wu, P., Ding, Y., Liu, Y., Li, X.: The characteristics of moisture recycling and its impact on regional precipitation against the background of climate warming over Northwest China, Int. J. Climatol., 39, 5241-5255, https://doi.org/10.1002/joc.6136, 2019.

605   Xie, C., Li, M., Zhang, X.: Characteristics of summer atmospheric water resources and its causes over the Tibetan plateau in

recent 30 years, J. Nat. Resour., 29, 979-989, 2014. (in Chinese with English abstract)

Xu, H., Lan, J., Zhang, G., Zhou, X.: Arid Central Asia saw mid-Holocene drought, Geology, 47, 255-258, https://doi.org/10.1130/g45686.1, 2019.

Yang, Y., Feng, Z., Zhang, D., Lan, B., Ran, M., Wang, W., Sun, A.: Holocene hydroclimate variations in the eastern Tianshan Mountains of northwestern China inferred from a palynological study, Palaeogeogr. Palaeoclimatol. Palaeoecol., 564, 110184, https://doi.org/10.1016/j.palaeo.2020.110184, 2021.

Yu, G., Xue, B., Wang, S., Liu, J.: Chinese lakes records and the climate significance during Last Glacial Maximum, Chin. Sci. Bull., 45, 250-255, https://doi.org/10.3321/j.issn:0023-074X.2000.03.003,　2000. (in Chinese with English abstract)

Yukimoto, S., Adachi, Y., Hosaka, M., Sakami, T., Yoshimura, H., Hirabara, M., Tanaka, T. Y., Shindo, E., Tsujino, H., Deushi, M. A new global climate model of the Meteorological Research Institute: MRI-CGCM3: Model description and basic performance, J. Meteorol. Soc. Japan, 90, 23-64, https://doi.org/10.2151/jmsj.2012-a02, 2012.

Zhang, H., Yu, K., Zhao, J., Feng, Y., Lin, Y., Zhou, W., Liu, G.: East Asian Summer Monsoon variations in the past 12.5 ka: High-resolution δ^{18}O record from a precisely dated aragonite stalagmite in central China, J. Asian Earth Sci., 73, 162-175, https://doi.org/10.1016/j.jseaes.2013.04.015, 2013.

Zhang, J., Nottebaum, V., Tsukamoto, S., Lehmkuhl, F., Frechen, M.: Late Pleistocene and Holocene loess sedimentation in central and western Qilian Shan (China) revealed by OSL dating, Quat. Int., 372, 120-129, https://doi.org/10.1016/j.quaint.2014.12.054, 2015.

Zhang, J. and Lin, Z.: Climate of China, Wiley, New York, 1992.

Zhang, D., Chen, X., Li, Y., Ran, M., Yang, Y., Zhang, S., Feng, Z.: Holocene moisture variations in the arid central Asia: new evidence from the southern Altai mountains of China, Sci. Total Environ., 735, 139545, https://doi.org/10.1016/j.quaint.2014.12.054, 2020.

Zhang, D. and Feng, Z.: Holocene climate variations in the Altai Mountains and the surrounding areas: a synthesis of pollen records, Earth Sci. Rev., 185, 847-869, https://doi.org/10.1016/j.earscirev.2018.08.007, 2018.

Zhang, Q., Lin, J., Liu, W., Han, L.: Precipitation seesaw phenomenon and its formation mechanism in the eastern and western parts of Northwest China during the flood season, Sci. China Earth Sci., 62, 2083-2098, https://doi.org/10.1007/s11430-018-9357-y, 2019.

Zhao, Y., An, C., Mao, L., Zhao, J., Tang, L., Zhou, A., Li, H., Dong, W., Duan, F., Chen, F.: Vegetation and climate history in arid western China during MIS2: New insights from pollen and grain-size data of the Balikun Lake, eastern Tien Shan, Quat. Sci. Rev., 126, 112-125, https://doi.org/10.1016/j.quascirev.2015.08.027, 2015.